Two-dimensional structure of light harvesting complex II (LHII) from the purple bacterium *Rhodovulum sulfidophilum* and comparison with LHII from *Rhodopseudomonas acidophila*

Hugh Savage, Marek Cyrklaff, Guillermo Montoya, Werner Kühlbrandt and Irmgard Sinning*

Background: Within the membranes of photosynthetic bacteria, up to three types of light harvesting complexes (LHI, LHII, LHIII) are found. These complexes absorb photons and transfer the excitation energy to the photosynthetic reaction centre. The LH complexes comprise units that contain α and β polypeptides with associated pigment molecules.

Results: The structure of LHII complex from *Rhodovulum sulfidophilum* has been examined to a resolution of 7 Å using electron microscopy. The complex is a nonamer containing nine αβ subunits. These are arranged in two radially symmetric concentric cylinders, with the nine α chains positioned in the inner cylinder and the nine β chains forming the outer cylinder. The 18 transmembrane helices are readily observed in the projection maps, along with 18 additional peaks attributed to the pigment molecules.

Conclusions: The determination of more structures of LH complexes will uncover the full extent of the variability of the oligomerization states in different bacteria and also in the native membrane. The analysis of two-dimensional crystals allows a rapid determination of key structural features and the oligomeric state of the complex. Comparison of our structure determined by electron microscopy with the recently solved X-ray structure indicates that the results of the two methods are complementary.

Address: European Molecular Biology Laboratory, Postfach 102209, D-69012 Heidelberg, Germany.

*Corresponding author.

Key words: cryo-electron crystallography, energy transfer, LHII complex, membrane protein, two-dimensional crystallization

Received: **7 Dec 1995**
Revisions requested: **22 Dec 1995**
Revisions received: **15 Jan 1996**
Accepted: **19 Jan 1996**

Structure 15 March 1996, **4**:243–252

Introduction

The capture of light energy during the initial stage of bacterial photosynthesis is mediated by light-harvesting (LH) or antenna complexes, which are integral membrane proteins. The energy of the photons is then very rapidly transferred to the photochemical reaction centre (RC) where a charge separation followed by electron transport across the membrane takes place [1].

Within purple bacteria, between one and three types of LH complexes can be found. With respect to their absorption maxima, they are referred to as the B880 (LHI), B800–850 (LHII) and B800–820 (LHIII) complexes [2]. The pigments present consist of bacteriochlorophyll (Bchl) and carotenoid molecules. The LHI complexes are believed to be arranged in the membrane such that they are in the immediate proximity of the RC and have a fixed stoichiometry relative to it. In contrast, a variable number of LHII and LHIII complexes lie outside the central RC–LHI core structure.

In general, bacterial LH complexes comprise two polypeptides (α and β), each of approximately 50 residues. The membrane-spanning region of each chain has been predicted, from hydrophobicity profile analysis [3], to consist of 20–25 residues of α-helical character, a result which is supported by circular dichroism studies. Some bacteria have multiple genes for the LH polypeptides and the type of LHII complex synthesized changes according to the light conditions [4]. In a preliminary report, the presence of two genes for the β polypeptide in *Rhodovulum* (*Rhv.*) *sulfidophilum* was postulated [5]; however, Tadros *et al.* [6] showed later that there was only one. In LHII from *Rhv. sulfidophilum* the 850 nm peak shows a characteristic spectral shift to 829 nm upon treatment with the detergent lauryl-dimethylamine-*N*-oxide (LDAO) [6]. This shift is completely reversible upon salt treatment and is thought to be an ion effect on the local conformation around the B850 Bchl [7], and the presence of a cation-binding site in close proximity of B850 Bchl was suggested. In addition, an influence of detergent treatment on the B800 Bchl absorption has been described for *Rhodopseudomonas* (*Rps.*) *acidophila* and *Rhodobacter* (*Rb.*) *sphaeroides* [8].

After many years of expecting the LHII complex to be a hexamer [9], the X-ray structure of LHII from *Rps. acidophila* (strain 10050) revealed a very simple and elegant arrangement of nine αβ heterodimers, organized as a

concentric ring structure [10]. The B850 Bchl molecules and the carotenoid molecules are found between the concentric rings formed by the α helices, while the B800 Bchls lie between the outer ring of helices of the β subunits.

The structure of the LHI complex from *Rhodospirillum* (*R.*) *rubrum* has also been shown, from electron microscopy (EM) projection maps at 8.5 Å [11], to consist of a ring structure; however, it contains 16 αβ heterodimers (instead of nine), which form two concentric cylinders, with the Bchls lying between them in the ring. The size of the hole in the centre is sufficiently large to accommodate the RC. EM studies on intact membranes from *Rps. viridis* [12,13], and also from *Ectothiorhodospira halochloris* [14], have shown that the ring formed by LHI actually surrounds the RC, although at that time it was thought that the ring contained only 12 αβ heterodimers. The actual arrangement of LHII in the membrane and also the arrangement of LHII and LHIII complexes with respect to LHI is not known.

In our previous report [15], we described the details of a new isolation protocol for LHII from the purple bacterium *Rhv. sulfidophilum* (formerly *Rhodobacter*) along with an initial analysis at low resolution (18 Å), obtained by EM from negatively stained two-dimensional (2D) crystals. In that study, the resolution was too low to reveal whether the LHII complex forms a heptamer, octamer or a higher oligomer. We have now collected higher resolution data to 7 Å, which shows unambiguously that the complex is a nonamer. We report here the details of this study and also a detailed comparison with the X-ray structure of *Rps. acidophila* (strain 10050) that has been reported recently [10].

Results and discussion

2D crystals

2D crystals of the tubular and vesicular type were obtained [15], with sizes of ~0.5×2–3 μm and 0.5×1–3 μm, respectively. Figure 1 shows a cryo-image of a vesicular crystal as used in the current analysis. In the previous low-resolution study [15], a different type of 2D crystal with $p42_12$ symmetry (a=b=157.0 Å) had been obtained. In the present study, a new crystal form is used which diffracts to higher resolution. The images clearly indicated an orthorhombic spacegroup with a=160.0 Å and b=140.0 Å. From an examination of the phase residuals using the program ALLSPACE [16], the spacegroup has been determined as $p22_12_1$, with four LHII complexes per unit cell. Figure 2 shows the Fourier transform of one of the best distortion-corrected images of a 2D LHII crystal. Reflections with IQ values of 3 are visible out to spacings of ~7 Å resolution (for definition of IQs, see Fig. 2). Table 1 shows the phase residuals and number of reflections obtained for the data averaged from four images, indicating the high quality of the phases to 7 Å resolution.

Projection maps

Projection maps of the unit cell were calculated. Figure 3a shows a projection map at 7 Å for the best image without symmetry being applied. The individual LHII complexes are organized in rings with an outer diameter of approximately 76 Å, similar to our previous data from tetragonal crystals [15] and to the X-ray structure [10]. After merging the data, the amplitudes were sharpened by the application of a resolution-dependent scale factor. A map calculated from these data, and with symmetry applied, is shown in Figure 3b. In both maps (a) and (b), a non-crystallographic ninefold symmetry is observable within each ring. Around the central hole, nine peaks representing the α subunits are seen, whilst on the outside a further nine peaks are present, corresponding to the β subunits.

Rotationally averaged map

One of the LHII complexes was cut out of the symmetrized projection map and rotationally averaged in reciprocal space (Fig. 4). The inner helices are almost perpendicular to the membrane plane, whereas the outer helices appear to be tilted. The distance between the centres of the peaks representing the individual inner helices is approximately 13 Å, whereas that between the outer helices is around

Figure 1

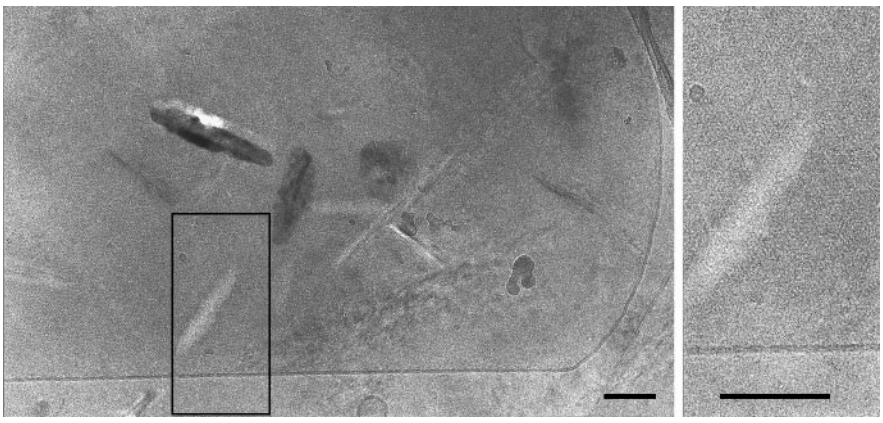

Unstained frozen-hydrated 2D crystals of the reconstituted LHII complex. The vesicular crystals obtained were between 1 and 3 μm in size. The area within the rectangular inset has been scaled up by a factor of two and is shown on the right-hand side of the figure. The length of the scale bar corresponds to 100 nm.

Figure 2

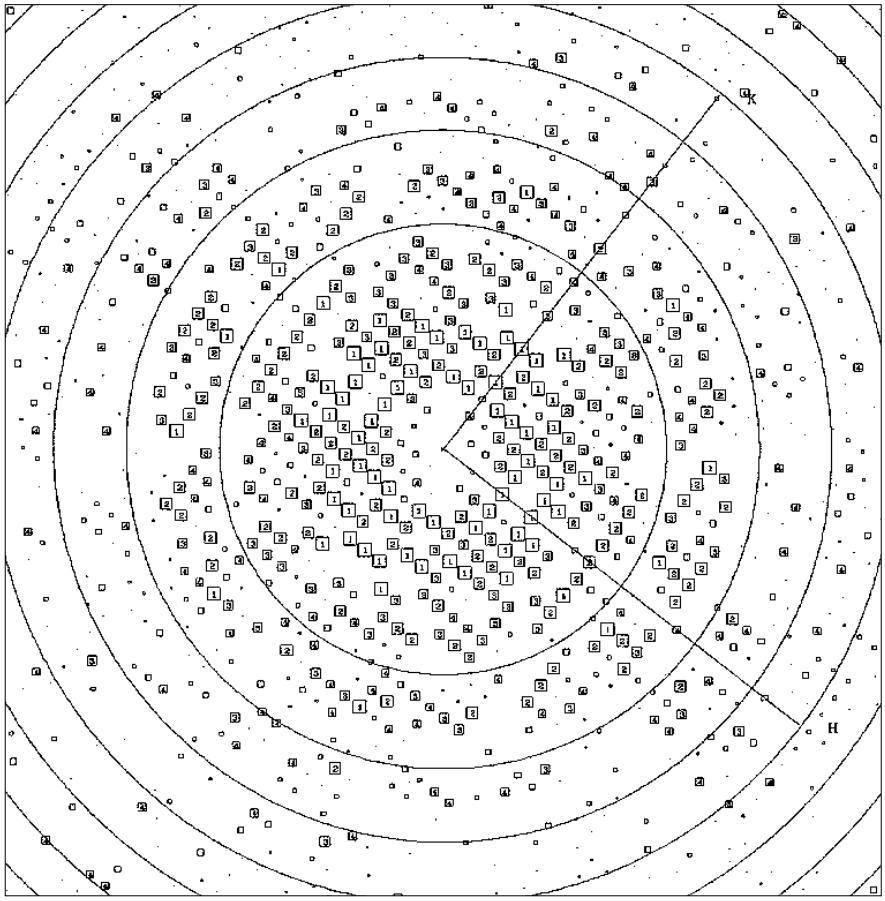

Fourier transform of the best image obtained from 2D crystals of LHII complexes from *Rhodovulum sulfidophilum*. The boxes indicate reflection positions and the size of the box refers to the IQ quality value of each spot. The IQ values are defined by 7/grade [28], where the grade refers to the signal-to-noise ratio of the reflection amplitudes. The lower the number, the higher the signal-to-noise ratio. The circles represent the zero values of the phase contrast transfer function and the axes give the directions of the reciprocal lattice vectors h and k. The resolution at the edge of the plot (i.e. the fourth circle) is approximately 6 Å, and it is approximately 4 Å in the corners.

23 Å; the two helices of one αβ heterodimer are separated by approximately 15 Å. A significant proportion of the density between the two rings of helices can be attributed to the 18 B850 Bchl molecules. The location of these molecules, close to the periplasmic surface of the membrane, and orientation of the tetrapyrrole macrocycles, perpendicular to the membrane plane, has been suggested previously from spectroscopic measurements [17]. In Figure 4, there is no obvious density for the nine B800 Bchl molecules, which have the tetrapyrrole macrocycles oriented parallel to the membrane plane, thus contributing less density to the projection map. Spectroscopic measurements suggest that there is one carotenoid molecule for every two Bchls [18]. The positions of the carotenoids could not be resolved in the 7 Å projection map.

Table 1

Distribution of phase errors against 0° or 180° and figures of merit, in resolution shells. All data with IQs of 1–5 are included.

Resolution shell (Å)	No. of F_{obs}	Mean value of $\Delta\alpha_c$ (°)*	No. of standard deviations of the mean below random (45°)	Mean figure of merit†
200.0–22.5	30	3.9	50.7	0.98
22.5–16.0	23	14.9	9.4	0.89
16.0–13.5	21	16.2	6.2	0.86
13.5–11.5	19	7.5	21.6	0.96
11.5–10.0	26	10.3	11.7	0.93
10.0–8.5	23	16.6	6.9	0.89
8.5–7.0	20	30.0	2.2	0.74
7.0–4.0	10	35.1	1.4	0.70
200.0–7.0	162	13.5	21.0	0.90

*$\Delta\alpha_c$ is defined as given by Bullough an Tulloch [34] as the difference between the symmetry-imposed phase of 0° or 180° and the observed phase. A value of 45° is random. †Figure of merit was calculated using a program kindly provided by P Bullough (unpublished program), in which it is given as $\cos(\Delta\alpha_c)$.

Comparison with LHI from *R. rubrum*

On comparing the EM projection map of Figure 4 with the corresponding 8.5 Å projection map of LHI from *R. rubrum* [11], it is apparent that there is less density between the outer helices in LHI, whereas in LHII the density is extended. As LHI does not contain B800 Bchls, the additional density can be attributed to these molecules. The two B880 Bchl molecules in the LHI complex could not be resolved as indicated by the presence of only one electron density peak between the helical peaks of the α and β subunits [11].

Figure 3

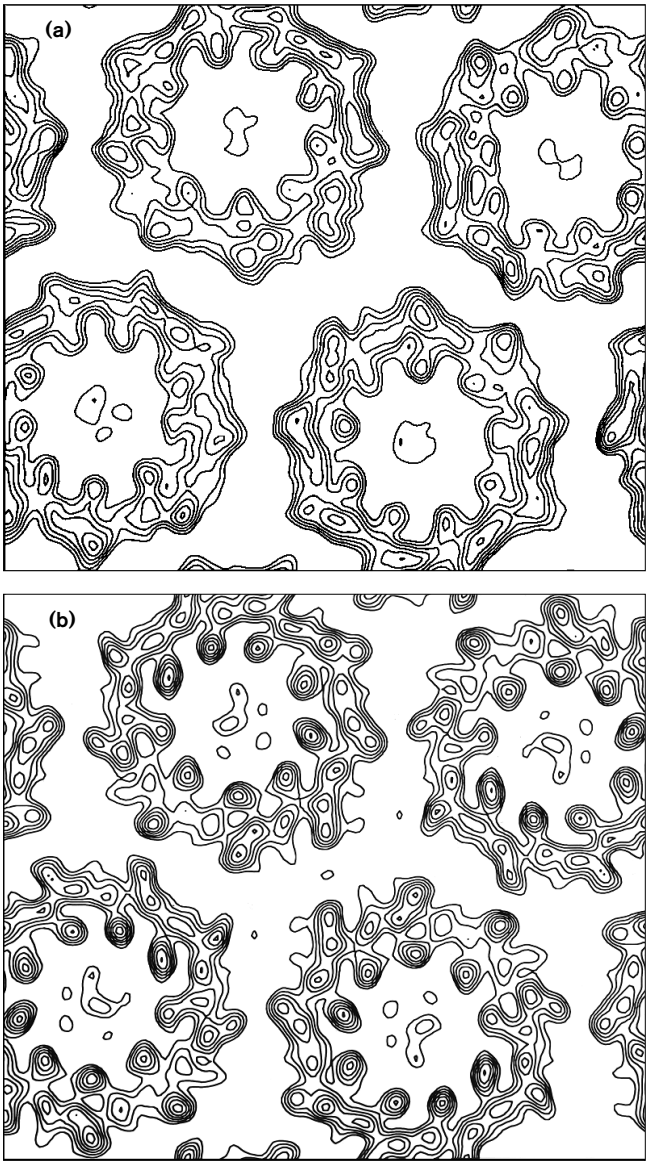

EM projection maps of LHII (B800–850) complex from *Rhv. sulfidophilum* calculated at 7 Å resolution from the processed images. **(a)** p1 projection map using Fourier coefficients and phases from the best image. One unit cell (a=160.0 Å, b=140.0 Å) is shown with the outer box representing the a (vertical) and b (horizontal) axes. No symmetry is applied. **(b)** Projection map calculated from Fourier coefficients and phases averaged from four images with the crystallographic $p22_12_1$ symmetry applied. The density is sharpened by applying a resolution-dependent scale factor to the amplitudes. As in (a), one unit cell is shown. The non-crystallographic ninefold rotational symmetry is clearly visible.

Figure 4

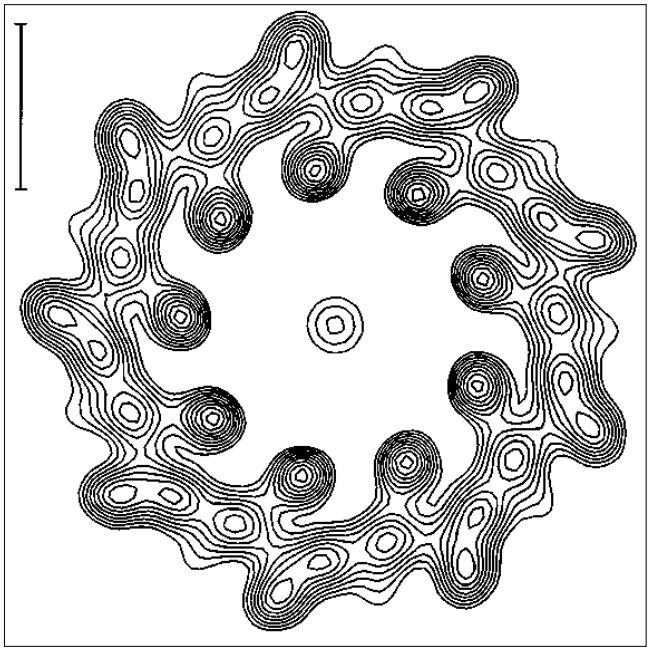

A rotationally filtered projection map is shown for one particle excised from Figure 3b. The inner and outer rings each contain nine peaks, representing the helices of the α (inner) and β (outer) subunits. Between the two rings, two further peaks are present which represent the Bchl and carotenoid molecules. However, the individual pigment molecules are not resolved. The scale bar drawn corresponds to 20 Å.

In addition, there are some significant differences in the relative positions of the helices in the two complexes. The distance between the helices of the α subunits in LHI is about 15 Å, compared with 13 Å in LHII. However, the separation of the outer helices of the β subunits is smaller in LHI, about 20 Å, compared with 23 Å for LHII. This reciprocal difference is probably due to the different number of αβ subunits present in each complex: LHI and LHII contain 16 and 9 αβ subunits, respectively. If the LHI complex was reduced to nine subunits then the inner ring of α subunits would become compressed, thus decreasing the inter α-subunit distances (from 15 Å to 13 Å), whereas the outer ring of β subunits would expand leading to an increase of the inter β-subunit distances (from 20 Å to 23 Å).

Comparison of the EM and X-ray structures

From the structural analysis of LHII from *Rps. acidophila* at 2.5 Å resolution, the interaction of the pigment molecules with the protein could be resolved in detail [10]. Clearly, this is not possible at 7 Å resolution. However, a detailed comparison of the X-ray structure with the EM structure at 7 Å resolution shows several major differences between the two LHII complexes. This comparison also allows a more detailed interpretation of the features observed in our EM projection map.

7 Å projection map of *Rps. acidophila* LHII complex

Using the model determined from X-ray analysis [10], a projection map, at 7 Å resolution, was calculated of the complete LHII complex of *Rps. acidophila* (Fig. 5a). In order to visualize the relative positions of the individual

Figure 5

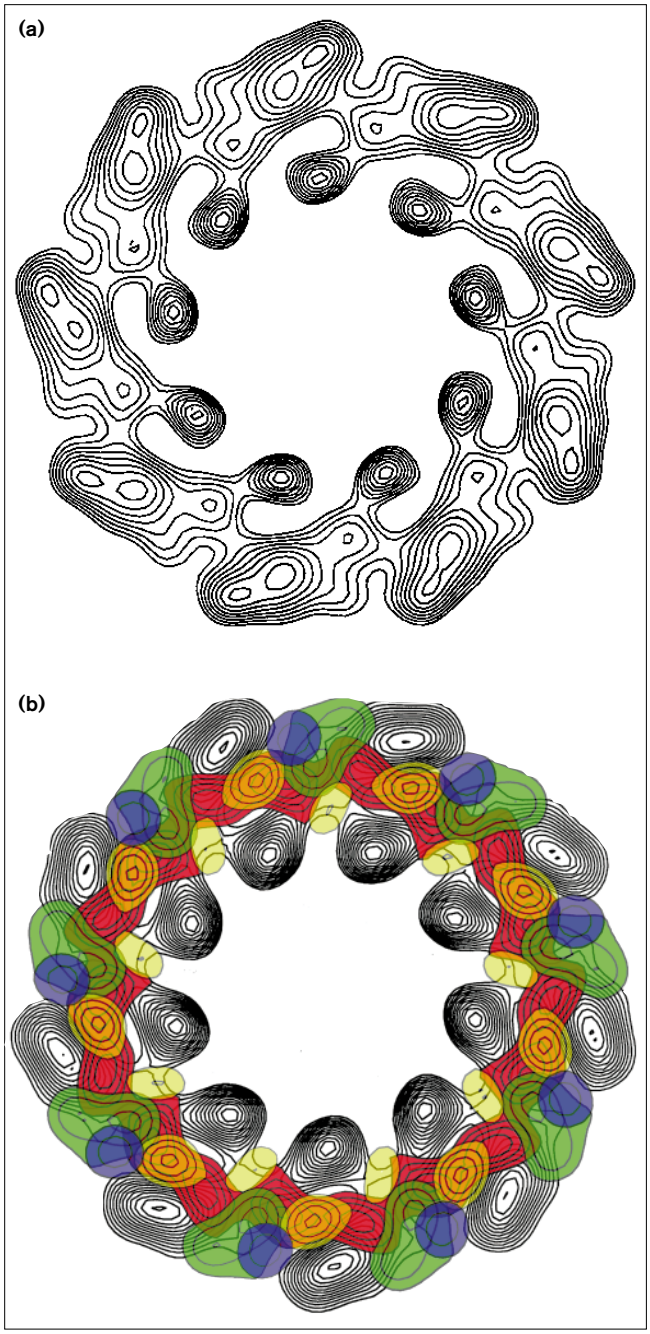

X-ray projection map for *Rps. acidophila* LHII complex at 7 Å resolution calculated from structure factors obtained from the coordinates of the refined X-ray model [10]. **(a)** X-ray projection map including all components. **(b)** Composite X-ray map, in which projection maps of the following five components were calculated, superimposed over each other and aligned: helices only of αβ subunits (black); B850 (upper) bacteriochlorophylls (18 molecules; red); inner carotenoids (9 molecules; yellow); B800 (lower) bacteriochlorophyll (9 molecules; green); outer carotenoids (9 molecules; blue). The relative positions of the individual components can be seen clearly. The peaks for the pigment molecules overlap closely and therefore are unresolvable in a 7 Å projection map (compare with Fig. 4).

components more clearly, maps were calculated separately for the following components: protein only, B800 Bchls, B850 Bchls, inner carotenoids and outer carotenoids. The five maps were overlaid and the resulting colour-coded 'composite' map is shown in Figure 5b. The peaks for the pigment molecules are seen to be closely overlapping and are unresolvable at 7 Å resolution.

The LHII complex from *Rps. acidophila* strain 10050 is also a nonamer and comprises two concentric cylinders (representing the α and β subunits) of transmembrane helices with a ninefold non-crystallographic symmetry: nine equally spaced αβ heterodimers. The nine inner helices are almost parallel, to within 2°, to the ninefold axis, whereas the angle of inclination of the outer helices is 15°. The helices themselves do not interact with one another and the distances between the helix centres are the same as in *Rhv. sulfidophilum*. The majority of the space between the helices is occupied by the B850 Bchl, B800 Bchl and carotenoid molecules (see Fig. 5b). The 18 B850 Bchls form a complete ring between the inner and outer helices and are oriented with their porphyrin planes parallel to the ninefold axis. Nine B800 Bchl molecules are situated in the outer cylinder in the regions between the β helices. They are oriented with their porphyrin planes perpendicular to the ninefold axis. Comparing the density of the B850 Bchls with that of the B800 Bchl molecules using the same contouring level, it can be seen that the B850s give a higher electron density than the B800s due to their different orientation relative to the membrane plane. There are two sets of carotenoid molecules, an 'inner' and an 'outer' set. These molecules are interdigitated between the B850 and B800 Bchls. In the original paper [10], the interpretation of the electron density for the second carotenoid was uncertain, but it has now been confirmed (N Isaacs, personal communication). The presence of a second carotenoid per protein heterodimer is of special interest, as from spectroscopic measurements the carotenoid:Bchl ratio was determined to be 1:2 for most LHI and LHII complexes isolated so far [18], including *Rps. acidophila* and *Rhv. sulfidophilum* [15].

Comparison of EM and X-ray projection maps

Figure 6a shows a superposition of the projection maps obtained for *Rhv. sulfidophilum* (EM; Fig. 4) and *Rps. acidophila* (X-ray; Fig. 5a). In both projection maps the overall features are very similar, with each map containing the same number of peaks. The nine inner helices are seen to line up exactly; however, the nine outer helices appear to be slightly displaced, with the centres of their peaks only partially overlapping. This difference might be due to a different degree of tilt of the outer helices, or to the presence of an additional ten residues at the N terminus of the β subunit in *Rhv. sulfidophilum* (Fig. 7). The sequence homology between *Rhv. sulfidophilum* and *Rps. acidophila* is about 60% (see Fig. 7). The α and β subunits

from *Rhv. sulfidophilum* LHII contain 52 and 51 residues, respectively [6]. In *Rhv. sulfidophilum* the α subunit is only one residue shorter at the C terminus than in *Rps. acidophila* (strain 10050), but there are several striking differences between the two sequences. Features unique to the *Rhv. sulfidophilum* α subunit include a high methionine content (four methionines versus one in *Rps. acidophila*), the presence of a carboxyl group at the C terminus and the presence of one cysteine. *Rhv. sulfidophilum* is the only purple bacterium known so far that has a cysteine residue in the LHII complex. The carboxyl group could be part of a proposed cation-binding site, which might be involved in regulating the spectral shift of the 829 nm peak to 850 nm upon salt treatment [6].

The density between the αβ polypeptides comprises two main peaks that are slightly displaced between the two maps. In the EM map, these peaks were initially assigned as two B850 Bchl molecules. Figure 6b–d shows superpositions of the EM map of Figure 4 with the individual pigment components of the X-ray map. The superpositions illustrate that the two major peaks between the helices of the EM map mainly represent the B850 Bchls, with contributions from B800 Bchls and carotenoid molecules.

The displacement of the peak centres (Fig. 6a) might be explained by the B850 Bchls having different orientations in the two LHII complexes resulting from different protein environments. The density between the outer helices is less pronounced in the EM than in the X-ray map. This region corresponds to the B800 Bchl molecules and the outer carotenoid molecules, which are shown as green and blue densities, respectively, in Figure 5b. The reason for this difference could also relate to the B800 Bchl molecules being oriented differently in the two structures, or it could reflect the absence or lower occupancy of the 'outer' carotenoid. The carotenoid:Bchl ratio was estimated as 1:2, using the standard extraction method [15].

Differences have been expected between the two structures of LHII from *Rps. acidophila* and *R. molischianum* in the tilt angle of the Bchls relative to the membrane plane [19]. The LHII complex of the latter is an octamer [20]. This has been confirmed in the recently determined 2.4 Å X-ray structure of the *R. molischianum* complex (H Michel, personal communication).

There is a methionine at the N terminus of the α subunit in the majority of LHII and LHI complexes. In *Rps. acidophila*,

Figure 6

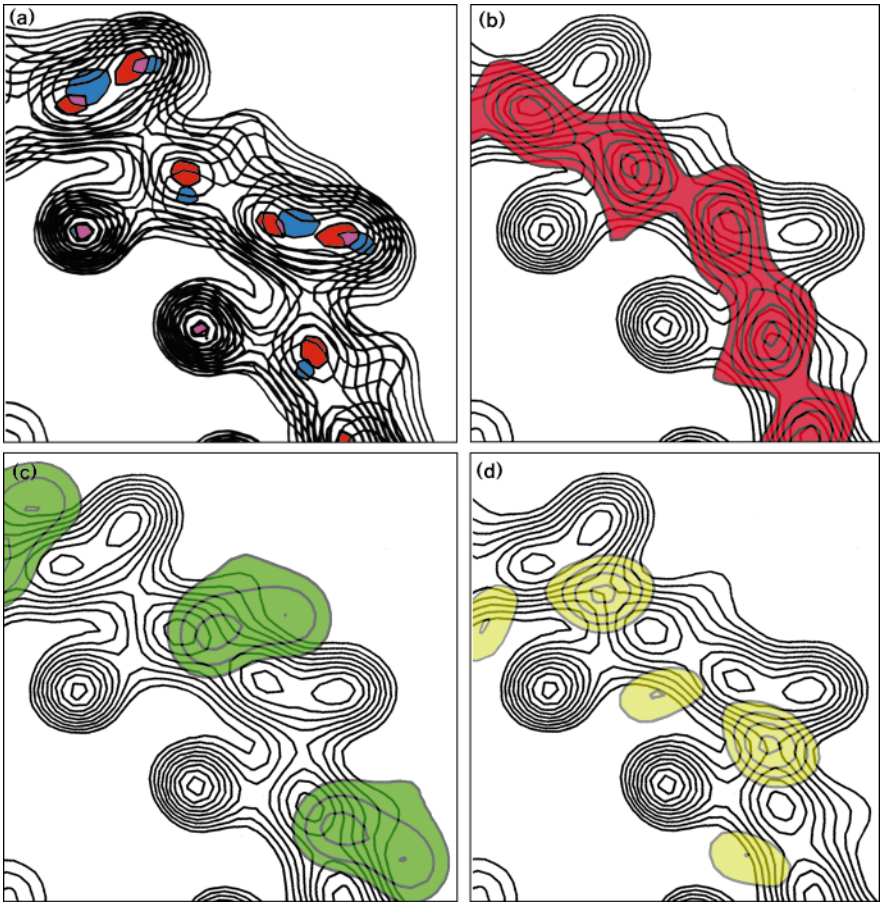

Comparison of the X-ray and EM projection maps. **(a)** Superposition of X-ray and EM maps. Peak centres are coloured red (EM) and blue (X-ray). **(b)–(d)** Superposition of the individual X-ray components (from Fig. 5b) with the EM map (from Fig. 4):
(b) B850 bacteriochlorophylls;
(c) B800 bacteriochlorophylls;
(d) inner carotenoids.

Figure 7

Amino acid sequences of the α and β polypeptide chains from a range of purple bacteria: **(a)** *Rhodovulum sulfidophilum* B800–850 [16]; **(b)** *Rhodopseudomonas acidophila* Ac10050 B800–850; **(c)** *Rhodobacter sphaeroides* 2.4.1. B800–850; **(d)** *Rhodobacter capsulatus* B800–850; **(e)** *Rhodospirillum molischianum* DSM 119 B800–850; (sequences (b)–(e) from [21]). The lines below sequences (d) and (e) show the conservation of the residues between the four sequences (a)–(d) and all five sequences, respectively. Exact homology is shown by =, and – represents conservative homology. The last line gives the secondary structure, which is based on the known X-ray structure of sequence (b). The number 3 represents a 3_{10} helix, H is an α helix. The long helices from residues 11–36 in the α subunit and 21–46 in the β subunit are the membrane-spanning helices.

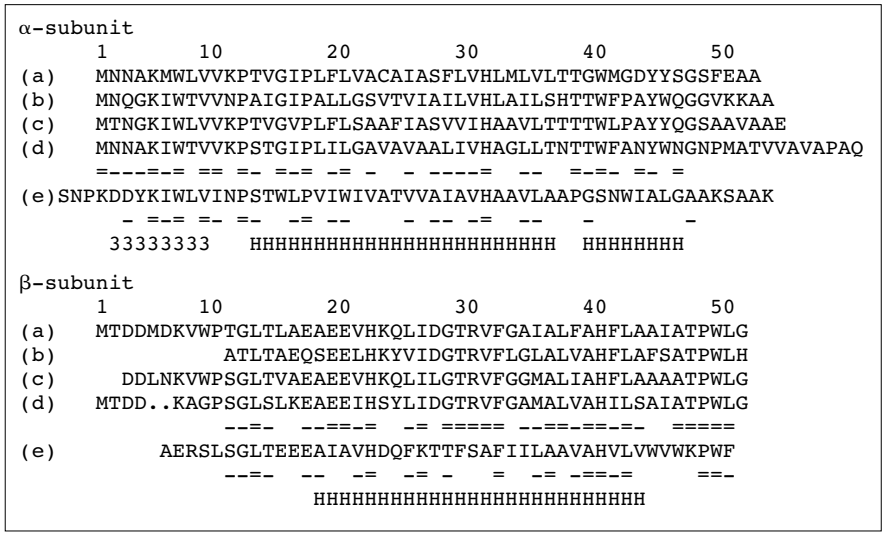

this methionine is liganding the magnesium ion of B800 [10]. The presence of methionine in *Rhv. sulfidophilum* suggests the presence of the same interaction. In *R. molischianum* the methionine is replaced by a serine at the N terminus. In addition, on the basis of spectroscopic measurements, LHII of *R. molischianum* was reported to show greater similarity to LHI rather than LHII complexes from other purple bacteria [21]. A sequence comparison (Fig. 7; and more detailed in [21]) also shows that LHII from *R. molischianum* shares more similarity with LHI than LHII complexes.

We have to await the determination of more structures of other bacterial antenna complexes in order to see whether different oligomerization states are present in different bacteria and the degree of variability. Already, one example of a different oligomer arrangement has been found: LHII from *R. molischianum* is an octamer (H Michel, personal communication). To date it is not known whether other lower or higher oligomers exist. The octamer form could be typical for those LHII complexes that are more closely related to LHI, as reported for *R. molischianum* [21]. In addition, no data are currently available on the assembly state of LHII in the native membrane. However, on the basis of the X-ray structure, which reveals details of how the pigments are interacting with the protein [10], it seems unlikely that this complex could change its oligomerization state upon detergent treatment. In 2D crystals the protein is in a lipid environment that is closer to that of the native membrane than the detergent micelle present in 3D crystals. Therefore, the fact that a ring-like structure of the same dimensions was obtained by X-ray and EM methods strongly suggests that this is a native and functional form of the complex and is not due to rearrangement in detergent. In the photosynthetic membrane, a random arrangement of LHII 'doughnuts' around the core complex of LHI and RC has been proposed by Kühlbrandt [22]. Although this seems a likely model, there is as yet no direct experimental evidence showing how the two complexes interact in the membrane.

As the same building principle is used for LHI and LHII complexes it seems likely that LHIII also has a similar structure. This additional complex can be found in some bacteria when grown under special light conditions. LHIII also consists of two polypeptides. The LHIII complex crystallizes in the same spacegroup, with similar cell parameters [23] to those found for LHII from *Rps. acidophila* [10], suggesting that it probably has the same concentric ring-type structure.

The fact that LHII from purple photosynthetic bacteria forms both 3D crystals diffracting X-rays to high resolution and 2D crystals amenable to electron crystallography, has enabled the most detailed comparison yet of a macromolecular structure determined by the two techniques. Previous comparisons have used EM data to about 17 Å only [24]. The structures are very similar, even though not only the crystals themselves but also the radiation applied to them was very different. The speed and relative ease of direct phase determination by image processing of 2D crystals is an important advantage of electron crystallography. But given well-ordered 3D crystals, it is still much easier to determine a protein structure by X-ray crystallography if the phase problem can be overcome. In future, the two methods may complement one another in solving intractable crystal structures, by using a map determined at moderate resolution by EM as an initial phasing model.

Biological implications

Photosynthesis is a fundamental process in the production of energy within organisms, and is readily exploited in plants and bacteria. The process involves the initial collection of solar energy and its conversion into chemical energy. Within photosynthetic bacteria, this is achieved using two different types of protein–pigment complexes that are present in the bacterial membranes. The first are called light-harvesting (antenna) complexes (LHI, LHII and LHIII); these are able to collect the incoming light and then deliver the excitation energy to the second type, the photosynthetic reaction centres (RC), where a charge separation occurs. Once we understand the molecular mechanisms and atomic structures of the membrane proteins involved in this fundamental process, we might be able to exploit photosynthesis as a renewable energy source. The first high-resolution structure of a bacterial antenna complex (LHII [10]) is now available, ten years after the structure of the bacterial RC was solved [25]. With the determination of low-resolution projection structures of LHI [11] and LHII (this work), the picture is becoming more complete. We are now able to follow bacterial photosynthesis at almost the atomic level.

All of the structures of bacterial LH complexes that have been solved appear to follow the same general building principle. They consist of two polypeptides (α and β) of about 50 amino acid residues. Pigment molecules (bacteriochlorophyll [Bchl] and carotenoid) are bound to the polypeptides and are responsible for the characteristic colour of the complex. We were able to show that the overall structural arrangement of LHII in *Rhodovulum* (*Rhv.*) *sulfidophilum*, determined by electron microscopy (EM), is very similar but not identical to the X-ray structure of *Rhodopseudomonas* (*Rps.*) *acidophila* [10]. The differences between these LHII structures might well be explained by differences in the polypeptide sequences. For example, the β subunit of *Rhv. sulfidophilum* has an additional 10 residues at the N terminus, which might form two turns of an α helix that lies on the membrane surface.

The ring-like arrangement of the αβ heterodimers of LHII is an elegant and simple construction to allow delocalization of the excitation energy and its very efficient transfer to LHI and the RC [7]. Positioning the Bchls in a slightly different protein environment in the different LH complexes is an ingenious way of tuning their absorption spectrum in order to extend the spectral range of light that can be used. Furthermore, the detailed comparison of the LHII complex from *Rhv. sulfidophilum* with the X-ray structure of *Rps. acidophila* [10] showed that the nonamer arrangement is present in different bacteria. Also, more importantly, it showed that the assemblies found in the 3D crystals are not artifacts of the crystallization procedure involving detergent extraction of the complex from the membrane. Important insights should be provided by the determination of the oligomeric states of other LH complexes, as although octamer and nonamer complexes have been identified there might be a greater variability than we currently imagine.

X-ray and electron crystallography are complementary techniques and as a number of membrane proteins are more likely to produce 2D rather than 3D crystals, comparative studies, like the one presented here, are very valuable aids in interpreting low-resolution images of structures. Furthermore, lower-resolution EM structures might be useful for the phasing of X-ray intensities when no other phase information is available.

Materials and methods

Purification and crystallization

Cells of *Rhv. sulfidophilum* DSM 1374 were grown and the LHII complex purified as described by Montoya *et al.* [15]. The 2D crystallization procedure was developed from that used for 3D crystals. A ratio of 70:1 of lipid to protein was found to be optimal in producing well ordered crystalline arrays. The protein concentration was 1 mg ml^{-1}. Samples were taken every few days and examined by electron microscopy. Large 2D crystals that were well ordered appeared within seven days of dialysis [15].

Cryo-electron microscopy

Samples for cryo-electron microscopy were prepared using the fully-hydrated method as described by Adrian *et al.* [26], with some modifications. Briefly, a 3 μl aliquot of crystal suspension was put on the carbon side of a holey carbon grid and then removed by micropipetting from the grid side (a modification of the procedure described by Toyoshima [27]). After repeating this procedure a few times, the excess liquid was removed by blotting with filter paper. The grids were frozen rapidly in liquid ethane at a temperature of about 93 K (–180°C) and stored in liquid nitrogen [28].

The grids were warmed up to 163 K (–110°C) in the electron microscope and imaged after the temperature stabilized at 100 K (–173°C), in order to convert amorphous ice to more rigid cubic ice [29]. This treatment was applied in order to improve the resolution of the images by providing a stronger support for the thin aqueous film, reducing beam-induced specimen movements.

Data collection and image processing

The grids were mounted in cryo-specimen holders (Oxford Instruments, CT-3500 Cryo-Transfer System) and observed in the JEOL 2000EX electron microscope operating at 200 kV accelerating voltage, equipped with a LaB_6 cathode and a liquid helium cooled twin-blade anticontaminator. Images of fully hydrated tubes and vesicles were recorded using low-dose conditions at nominal magnifications of 40 000 and 60 000 with an exposure time of 1 s, resulting in an electron dose of 4–8 e $Å^{-2}$ at the specimen. Underexposed micrographs were recorded on Kodak SO–163 EM film and developed in full strength Kodak D-19 for 12 min at room temperature. Optical diffraction was used to assess image quality and select the best images. Areas of 4000×4000 pixels were digitized on a Perkin-Elmer 1010M flat-bed microdensitometer with a circular aperture of 10 μm at a step size of 8 μm, corresponding to a pixel size of 2 Å (40 000×) or 1.33 Å (60 000×) at the specimen.

Two superimposed lattices, each generated by one side of a collapsed tube or vesicle, were observed. The lattices were easily separated as they were rotated by ~30° with respect to one another. The images were processed using the MRC image processing package [30]. Indexing revealed that the planar unit cell was orthorhombic with cell parameters of a=160.0 Å and b=140.0 Å, which were seen to be different from the previously observed crystals, which had a square unit cell of a=b=157.0 Å.

Images were corrected for small distortions of the 2D lattice, contrast transfer and objective lens astigmatism [31,32]. After corrections, an internal comparison of structure factor phases was made using the program ALLSPACE [16]. In total, 12 images were processed and the four best ones were chosen for merging. For each of the four images processed, the best phase residual indicated that the planar space-group was $p22_12_1$. The phase origin of each image was refined and the images merged using ORIGTILTB. Table 1 shows a comparison of the phase errors in different resolution shells. The program SCALIMAMP3D (R Henderson, unpublished program) was used to apply a resolution dependent scale factor to the merged data set, by comparison of the amplitudes to a reference data set, from bacteriorhodopsin [33].

Map calculations and averaging

The CCP4 suite of crystallographic programs was used to calculate Fourier projection maps using the corrected and averaged amplitudes and phases [34]. As the projection is centrosymmetric, phases were set to 0° or 180°. Electron-density maps were calculated in which $p22_12_1$ symmetry was applied. One of the ring-like complexes was extracted from the map and a Fourier analysis of its power spectrum undertaken [35]. Using the extracted map segment, a rotationally filtered projection map was synthesized using the program RFILTIM [34], with a ninefold rotational component (40% of the azimuthal power).

X-ray map calculations

Coordinates from the 2.5 Å X-ray structure of *Rps. acidophila* strain 10050, kindly provided by Prof N Isaacs, were used to compare the EM and X-ray structures. Firstly, an X-ray projection map of the whole complex was computed to a resolution of 7 Å using calculated structure factors (Fig. 5a). At the same resolution, several projection maps for individual components of the complex were also calculated, showing separate projections of the αβ helical subunits, B850 Bchls, B800 Bchls, inner carotenoids and outer carotenoids. The five individual maps were then aligned and superimposed graphically to form a 'composite' map which is illustrated in Figure 5b. In addition, the B850s, the B800s and the inner carotenoids where superimposed separately onto the EM rotationally averaged projection map of Figure 4. These respective maps are shown in Figure 6b–d and compared with the EM maps in the results and discussion section.

Acknowledgements

We are very grateful to Prof N Isaacs of Glasgow University (UK) for kindly giving us a set of coordinates for the X-ray structure of the *Rhodopseudomonas acidophila* LHII complex. We thank Prof Richard Henderson and Dr Per Bullough for their help and discussions in the application of the SCALIMAMP3D and rotational averaging programs, and also Cecilia Svensson for providing excellent technical assistance. GM was supported by an EU fellowship.

References

1. van Grondelle, R., Dekker, J.P., Gillbro, T. & Sundstrom, V. (1994). Energy transfer and trapping in photosynthesis. *Biochim. Biophys. Acta* **1187**, 1–65.
2. Zuber, H. & Brunisholz, R.A. (1991). Structure and function of antenna polypeptides and chlorophyll–protein complexes: principles and variability. In *Chlorophylls* (Scheer, H., ed.), pp. 669–672, CRC Press, Boca Raton, FL.
3. Zuber, H. (1985). Structure and function of light harvesting complexes and their polypeptides. *Photochem. Photobiol.* **42**, 821–844.
4. Tadros, M.H. & Waterkamp, K. (1989). Multiple copies of the coding regions for the light-harvesting B800-850 α- and β-polypeptides are present in the *Rhodopseudomonas palustris* genome. *EMBO J.* **8**, 1303–1308.
5. Doi, M. & Mäntele, W. (1992). Protein structure of the light-harvesting pigment-protein complexes isolated from *Rb. sulfidophilus*. In *Research in Photosynthesis*. (Murata, N., ed.), vol. **1**, pp. 49–52, Kluwer Academic Publishers, The Hague, Netherlands.
6. Tadros, M.H., Hagemann, G.E., Katsiou, E., Dierstein, R. & Schiltz, E. (1995). Isolation and complete amino acid sequence of the β- and α-polypeptides from the peripheral light-harvesting pigment–protein complex II of *Rhodobacter sulfidophilus*. *FEBS Lett.* **368**, 243–247.
7. Mäntele, W., Sawatzki, J., Doi, M., Gadón, N. & Drews, G. (1991). Bacteriochlorophyll–protein interaction in the light-harvesting complex B800–850 from *Rhodobacter sulfidophilus*: A Fourier-transform Raman spectroscopic investigation. *Biochim. Biophys. Acta*, **1057**, 367–372.
8. Doi, M., Yuzo, S., Gadón, N., Golecki, J.R. & Drews, G. (1991). Spectroscopical studies on the light-harvesting pigment–protein complex II from dark-aerobic and light-anaerobic grown cells of *Rhodobacter sulfidophilus*. *Biochim. Biophys. Acta* **1058**, 235–241.
9. Papiz, M.Z., *et al.*, & Lindsay, J.G. (1989). Crystallization and characterization of two crystal forms of the B800–850 light-harvesting complex from *Rhodopseudomonas acidophila* strain 10050. *J. Mol. Biol.* **209**, 833–835.
10. McDermott, G., *et al.*, & Isaacs, N.W. (1995). Crystal structure of an integral membrane light-harvesting complex from photosynthetic bacteria. *Nature* **374**, 517–525.
11. Karrasch, S., Bullough, P.A. & Ghosh, R. (1995). 8.5 Å projection map of the light-harvesting complex I from *Rhodospirillum rubrum* reveals a ring composed of 16 subunits. *EMBO J.* **14**, 631–638.
12. Stark, W., Kühlbrandt, W., Wildhaber, H., Wehrli, E. & Mühlethaler, K. (1984). The structure of the photoreceptor unit of *Rhodopseudomonas viridis*. *EMBO J.* **3**, 777–783.
13. Miller, K.R. (1982). Three-dimensional structure of a photosynthetic membrane. *Nature* **300**, 53–55.
14. Engelhardt, H., Engel, A. & Baumeister, W. (1986). Stoichiometric model of the photosynthetic unit of *Ectothiorhodospira halochloris*. *Proc. Natl. Acad. Sci. USA* **83**, 8972–8976.
15. Montoya, G., Cyrklaff, M. & Sinning, I. (1995). Two-dimensional crystallisation and preliminary structure analysis of light harvesting II (B800-850) complex from the purple bacterium *Rhodovulum sulfidophilum*. *J. Mol. Biol.* **250**, 1–10.
16. Valpuesta, J.M., Carrascosa, J.L. & Henderson, R. (1994). Analysis of electron microscope images and electron diffraction patterns of thin crystals of ∅29 connectors in ice. *J. Mol. Biol.* **240**, 281–287.
17. Kramer, H.J.M., van Grondelle, R., Hunter, C.N., Westerhuis, W.H.J. & Amesz, J. (1984). Pigment organization of the B800–850 antenna complex of *Rhodopseudomonas sphaeroides*. *Biochim. Biophys. Acta* **765**, 156–165.
18. Hawthornthwaite, A.M. & Cogdell, R.J. (1993). Bacteriochlorophyll-binding proteins. In *Chlorophylls.* (Scheer, H., ed), pp. 493–528, CRC Press, Boca Raton, FL.
19. Hu, X., Xu, D., Hamer, K., Schulten, K., Koepke, J. & Michel, H. (1995). Predicting the structure of the light-harvesting complex II of *Rhodospirillum molischianum*. *Protein Sci.* **4**, 1670–1682.
20. Kleinekofort, W., Germeroth, L., van den Broek , J.A., Schubert, D. & Michel, H. (1992). The light-harvesting complex II (B800/B850) from *Rhodospirillum molischianum* is an octamer. *Biochim. Biophys. Acta* **1140**, 102–104.
21. Germeroth, L., Lottspeich, F., Robert, B. & Michel, H. (1993). Unexpected similarities of the B800–850 light-harvesting complex from *Rhodospirillum molischianum* to the B870 light-harvesting complex from other purple photosynthetic bacteria. *Biochemistry* 32, 5615–5621.
22. Kühlbrandt, W. (1995). Structure and function of bacterial light-harvesting complexes. *Structure* **3**, 521–525.
23. Guthrie, N., *et al.*, & Lindsay, J.G. (1992). Crystallisation of the B800–820 light-harvesting complex from *Rhodopseudomonas acidophila* strain 7750. *J. Mol. Biol.* **224**, 527–528.
24. Voges, D., *et al.*, & Huber, R. (1994). Three-dimensional structure of the membrane-bound Annexin V : a correlative electron microscopy-X-ray crystallography study. *J. Mol. Biol.* **238**, 199–213.
25. Deisenhofer, J., Epp, O., Miki, K., Huber, R. & Michel, H. (1985). Structure of the protein subunits in the photosynthetic reaction centre of *Rhodopseudomonas viridis* at 3 Å resolution. *Nature* **318**, 618–624.
26. Adrian, M., Dubochet, J. & McDowall, A.W. (1984). Cryo-electron microscopy of viruses. *Nature* **308**, 32–36.
27. Toyoshima, C. (1989). On the use of holey grids in electron crystallography. *Ultramicroscopy* **30**, 439–444.

28. Cyrklaff, M, Auer, M., Kühlbrandt, W. & Scarborough, G.A. (1995). 2D structure of the *Neurospora crassa* plasma membrane ATPase as determined by electron cryomicroscopy. *EMBO J.* **14**, 1854–1857.
29. Cyrklaff, M. & Kühlbrandt, W. (1994). High-resolution electron microscopy of biological specimens in cubic ice. *Ultramicroscopy* **55**, 141–153.
30. Henderson, R., *et al*., & Downing, K.H., (1990). Model for the structure of bacteriorhodopsin based on high-resolution electron cryo-microscopy. *J. Mol. Biol.* **213**. 899–929.
31. Henderson, R., Baldwin, J., Downing, K.H., Lepault, J. & Zemlin, F. (1986). Structure of purple membrane from *Halobacterium halobium*: recording, measurement and evaluation of electron micrographs at 3.5 Å resolution. *Ultramicroscopy* **19**, 147–178.
32. Havelka, W.A., Henderson, R., Heymann, J.A.W. & Oesterhelt, D. (1993). Projection structure of halorhodopsin from *Halobacterium halobium* at 6 Å resolution obtained by electron cryo-microscopy. *J. Mol. Biol.* **234**, 837–846.
33. Schertler, G.F.X., Villa, C. & Henderson, R. (1993). Projection structure of rhodopsin. *Nature* **362**, 770–772.
34. Bullough, P.A. & Tullock, P.A. (1991). High resolution spot-scan electron microscopy of microcrystals of an α-helical coiled-coil protein. *J. Mol. Biol.* **215**, 161–173.
35. Crowther, R.A. & Amos, L.A. (1971). Harmonic analysis of electron microscope images with rotational symmetry. *J. Mol. Biol.* **60**, 123–130.